Modeling Anisoplanatism in the Keck II Laser Guide Star AO System

Michael P. Fitzgerald[a], Gunther Witzel[a], Matthew C. Britton[b], Andrea M. Ghez[a],
Leo Meyer[a], Breann N. Sitarski[a], Carina Cheng[a], Eric E. Becklin[a], Randall D. Campbell[c],
Tuan Do[d], Jessica R. Lu[e], Keith Matthews[f], Mark R. Morris[a], Christopher R. Neyman[c],
Glenn A. Tyler[b], Peter L. Wizinowich[c], and Sylvana Yelda[a]

[a]Department of Physics & Astronomy, University of California, Los Angeles, 430 Portola
Plaza. Box 951547, Los Angeles, CA, 90095-1547;
[b]the Optical Sciences Company, 1341 South Sunkist St., Anaheim, CA, 92806;
[c]W. M. Keck Observatory, 65-1120 Mamalahoa Hwy., Kamuela, HI, 96743;
[d]Department of Physics & Astronomy, University of California, Irvine, 4129 Frederick Reines
Hall, Irvine, CA 92697-4575;
[e]Institute for Astronomy, 2680 Woodlawn Drive, Honolulu, HI 96822-1839;
[f]Caltech Optical Observatories, California Institute of Technology, 1200 E. California Blvd.,
Pasadena, CA 91125

ABSTRACT

Anisoplanatism is a primary source of photometric and astrometric error in single-conjugate adaptive optics. We present initial results of a project to model the off-axis optical transfer function in the adaptive optics system at the Keck II telescope. The model currently accounts for the effects of atmospheric anisoplanatism in natural guide star observations. The model for the atmospheric contribution to the anisoplanatic transfer function uses contemporaneous MASS/DIMM measurements. Here we present the results of a validation campaign using observations of naturally guided visual binary stars under varying conditions, parameterized by the r_0 and θ_0 parameters of the C_n^2 atmospheric turbulence profile. We are working to construct a model of the instrumental field-dependent aberrations in the NIRC2 camera using an artificial source in the Nasmyth focal plane. We also discuss our plans to extend the work to laser guide star operation.

1. INTRODUCTION

Anisoplanatism arises in ground-based astronomical imaging because different lines of sight probe different columns of atmosphere above the entrance aperture. In single-conjugate adaptive optics imaging, this leads to a field-dependent aberrations, with greater degree of aberration at larger angles from the reference direction. Optical mitigation of anisoplanatism generally requires multi-conjugate (or multi-object) adaptive optics, significantly increasing the cost and complexity of the adaptive correction when compared to a single-conjugate system. Most telescopes today equipped with adaptive optics have only single-conjugate systems.

The field dependence of the anisoplanatic point-spread function (PSF) poses a challenge to accurate photometry and astrometry. As the PSF becomes increasingly blurred away from the wavefront reference direction, the energy encircled in a given aperture decreases. As a consequence, no single PSF reference observation can be used to derive photometric encircled energy corrections unless the field-dependence of PSF blurring is taken into account.[1] This has posed a significant barrier to photometry over even moderate field angles, for example in constructing color-magnitude diagrams of stellar clusters. Accounting for the field-dependent shape of the anisoplanatic PSF can also be important for astrometric measurements, such as those made in the region of the Galactic Center.

Further author information: (Send correspondence to M.P.F.)
M.P.F.: E-mail: mpfitz@ucla.edu, Telephone: 1 310 206 7853

Previous efforts at accounting for these effects have attempted to derive the field-dependence of anisoplanatism from imaging with the science camera.[2,3] Such approaches require either non-contemporaneous imaging compared to the science observations, or require crowded science fields. An alternative approach is to use measurements of the atmospheric turbulence profile $C_n^2(z)$ to forward model the field dependence of anisoplanatism; this technique has been demonstrated on-sky at Palomar Observatory.[4] This type of approach has the advantage of being contemporaneous with science observations that are not required to be of crowded fields.

In this article, we present the first results of our effort to use measurements of the atmospheric turbulence profile to forward-model anisoplanatism in natural guide star (NGS) adaptive optics imaging on Mauna Kea. We demonstrate the application of MASS/DIMM measurements of $C_n^2(z)$ to model the blurring of the on-axis PSF in order to reconstruct the off-axis PSF in a series of binary star measurements made with the NIRC2 camera. We also describe our ongoing work to account for instrumental field-dependent aberrations, as well as our future plans to extend this model to laser guide star (LGS) adaptive optics.

In most of the analysis that follows, it is often convenient to work with the optical transfer function (OTF), which is the Fourier transform of the point-spread function. Here, we consider the transfer functions corresponding to the time- and field-angle-variable PSF. The OTF is a function of spatial frequency $\boldsymbol{f}$, field angle $\boldsymbol{\alpha}$, and time t, and can be decomposed as

$$\text{OTF}(\boldsymbol{f}; \boldsymbol{\alpha}, t) = \text{OTF}_{\text{on}-\text{axis}}(\boldsymbol{f}; t) \cdot \text{OTF}_{\text{inst}-\text{off}}(\boldsymbol{f}; \boldsymbol{\alpha}, t) \cdot \text{OTF}_{\text{aniso}}(\boldsymbol{f}; \boldsymbol{\alpha}, t). \tag{1}$$

The OTF is approximated as independent contributions from an on-axis transfer function $\text{OTF}_{\text{on}-\text{axis}}$, an off-axis instrumental transfer function $\text{OTF}_{\text{inst}-\text{off}}$, and an atmospheric (anisoplanatic) transfer function $\text{OTF}_{\text{aniso}}$. In this work, "on-axis" refers to the location where the field angle $\boldsymbol{\alpha}$ is defined to be zero; such terminology will need to be revised for the future LGS case.

2. ANGULAR ANISOPLANATISM

2.1 The Anisoplanatic Transfer Function

Anisoplanatism introduces a time and field dependent variability in the image quality delivered by a natural guide star adaptive optics system. Figure 1 displays the origin of this effect for a natural guide star adaptive optics system. Due to the vertical extent of atmospheric turbulence, light from the guide star and light from the science target encounter different columns of atmospheric turbulence, yielding a difference in the phase aberrations between the wavefronts. This is the effect of angular anisoplanatism. The adaptive optics system senses and compensates phase aberrations in the wavefront of the guide star. The effect of the residual wavefront aberrations arising from anisoplanatism causes a degradation in image quality that increases with angular offset from the guide star due to the shearing of the two columns. The effect also depends on the vertical distribution of atmospheric turbulence, which evolves continuously in time. The resulting time and field dependence of the PSF presents significant challenges in applications for which quantitative measurements are required, such as differential photometry and astrometry in crowded fields.

Analytic expressions are available for the long exposure atmospheric structure function $D_{\text{aniso}}(\boldsymbol{r}_1, \boldsymbol{r}_2)$ associated with the effects of anisoplanatism in natural and laser guide star adaptive optics systems. In addition to the dependence on the pupil plane coordinates $\boldsymbol{r}_1$ and $\boldsymbol{r}_2$, this structure function depends on a number of parameters: the observing wavelength λ, the aperture diameter D, the angular offsets among the laser and/or natural guide stars and the science target, the zenith angle ζ, the vertical turbulence profile $C_n^2(z)$, and the range to laser guide star. With the exception of $C_n^2(z)$, these parameters are all deterministic quantities in an astronomical observation. A measurement of $C_n^2(z)$ permits an analytic determination of the long exposure structure function arising from atmospheric turbulence.

In the case of a natural guide star adaptive optics system, the long exposure structure function is stationary: $D_{\text{aniso}}(\boldsymbol{r}_1, \boldsymbol{r}_2) = D_{\text{aniso}}(\boldsymbol{r}_1 - \boldsymbol{r}_2)$. This simplification leads to the factorization of the optical transfer function indicated in Equation 1. Under these circumstances, the quantity $\text{OTF}_{\text{aniso}}(\boldsymbol{f}; \boldsymbol{\alpha}, t)$ may be computed directly from the long exposure atmospheric structure function for use in Equation 1.

Figure 1. Anisoplanatism in a Natural Guide Star Adaptive Optics System and the Siting of the MASS/DIMM on Mauna Kea. On the left is shown the columns of turbulence sampled by the guide star (blue) and a science target (green). Due to the vertical extent of atmospheric turbulence, light from the guide star and light from the science target encounter different columns of atmospheric turbulence, yielding a difference in the phase aberrations between the wavefronts. This is the effect of angular anisoplanatism. The effect depends on both the time-dependent vertical distribution of atmospheric turbulence and on angular offset from the guide star. Measurements of the vertical turbulence profile $C_n^2(z)$ may be performed using a MASS/DIMM unit currently in operation on Mauna Kea. The unit is located near the Canada France Hawaii Telescope, as indicated by the red dot in the image.

2.2 Turbulence Profile Measurement on Mauna Kea

An instrument to measure the vertical turbulence profile has been developed and deployed at the summit of Mauna Kea. This instrument contains a Differential Motion Monitor (DIMM) to measure the integrated atmospheric seeing and a Multiaperture Scintillation Sensor (MASS) to resolve vertical structure of the turbulence profile.[5] A robotic telescope equipped with a MASS/DIMM and originally developed for use in the Thirty Meter Telescope site testing campaign[6] has been deployed on the summit of Mauna Kea. Weather permitting, this unit tracks $m_V < 2$ stars and delivers seven-layer estimates of the vertical turbulence profile on ∼90 second intervals.

Data acquired with the MASS/DIMM unit are available via the internet from the Mauna Kea Weather Center website.[7] These data are available from 2009 September to present. On each night for which data have been acquired, two files are available. The first file contains timestamped measurements of the atmospheric seeing from the DIMM. The second file contains a six layer estimate of $C_n^2(z)$ plus the free atmospheric seeing. Data from these two files may be combined to yield a seven layer estimate of the turbulence profile. Measurements from the MASS and DIMM are not synchronous, and must be interpolated to form this estimate.

2.3 Construction of the Transfer Function

Software to compute the anisoplanatic transfer function and form estimates of the field dependent point-spread function has been developed for use on this program. The anisoplanatic transfer function for a natural guide star adaptive optics system $\mathrm{OTF}_{\mathrm{aniso}}(\boldsymbol{f}; \boldsymbol{\alpha}, t)$ may be computed analytically from the deterministic quantities λ, D, $\boldsymbol{\theta}_{ab}$, and ζ, and from a measurement of the vertical turbulence profile $C_n^2(z)$. Together with an estimate of the guide star transfer function, $\mathrm{OTF}_{\mathrm{on-axis}}(\boldsymbol{f}; t)$, and the instrumental transfer function, $\mathrm{OTF}_{\mathrm{inst-off}}(\boldsymbol{f}; \boldsymbol{\alpha}, t)$, Equation 1 yields an estimate of the field dependent optical transfer function for a natural guide star adaptive optics system. Fourier transformation of the optical transfer function yields the point-spread function.

We developed a C++ class library to read the MASS/DIMM files available from the Mauna Kea Weather Center and a NIRC2 file generated during observations at Keck to produce predictions of the field-dependent

PSF at the wavelength and zenith angle of the observation. This prediction may be performed using the ideal, diffraction limited Keck PSF, using an observation of the guide star from the NIRC2 field, or using a version of the guide star observation modified to account for the field dependent instrumental effects. A set of IDL plugins were developed so that this functionality may be called directly from an IDL shell.

3. BINARY STAR TESTS

3.1 Observations

Binary star systems are used as simple test cases for the predictive power of the atmospheric model described above. Here, as a first step, we concentrate on NGS observations, using the optically brighter star as a wavefront reference and testing the effects of differential aberrations with the companion star. A typical frame is shown in Fig. 2.
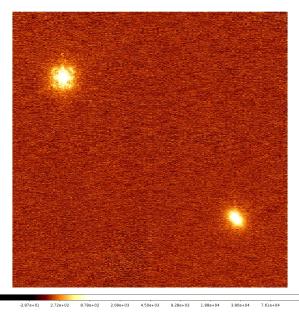

Figure 2. A single frame from the naturally guided observation of the binary CCDM 16242+3702 (8.2″ separation). The AO loop was closed on the star in the upper left. The companion star PSF shows a clear elongation towards the guide star due to angular anisoplanatism.

Between 2011 July and September, 8 NGS binary datasets were obtained with the NIRC2 narrow camera under a range of different atmospheric conditions as well as different orientations with respect to the pointing of the MASS/DIMM unit. NIRC2 is a facility camera for the adaptive optics system on the Keck II telescope; we used it in the "narrow" mode, which gives a $10''\times10''$ field at a sampling of $\sim10\,\mathrm{mas\,pix^{-1}}$. We chose binaries with separations between 6.6″ and 9.1″ and the FeII filter ($\lambda_c = 1.65\,\mu\mathrm{m}$) to maximize the differential atmospheric effects. From these datasets, we have selected two sets of binary star observations that have good signal-to-noise in both stars and that exhibit strong anisoplanatism (Figure 3). One of the binary stars, CCDM 22173-0042, was observed while the MASS/DIMM reference star was angularly nearby (at a separation of 4° on the sky). The other binary star, CCDM 16242+3702, was observed at a greater angular separation from the MASS/DIMM references; for the first 29 frames the MASS/DIMM reference used was 37° away, while the remaining frames were obtained with a different MASS/DIMM reference star, located 54° away. Each dataset covers a period of 20 to 44 minutes with comparatively stable atmospheric conditions. In both cases, the signal-to-noise of the fainter companion PSF is good enough to sample the most prominent features in the halo of the off-axis PSF. The datasets were obtained at different rotation angles in order to locate the stars in detector quadrants with low read noise contribution. Table 1 summarizes the observational details for these binary stars and the measured relative positions of their components.
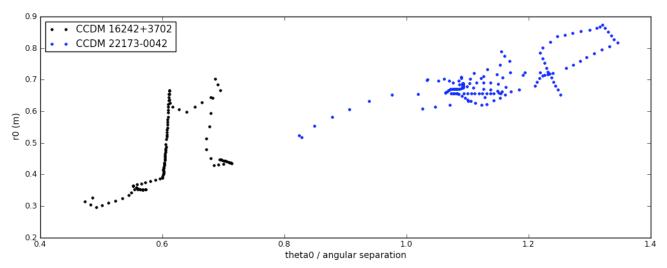
Figure 3. This figure shows the Fried-parameter r_0 vs. the isoplanatic angle θ_0 (normalized by the individual separation of the binary) for the binary test data in Table 1. These parameters are indicative for the degree of anisoplanatism in the individual dataset, and are referenced to the wavelength of observation. The isoplanatic angle θ_0 was on the order of the binary separation for these observations.

CCDM	UT Date	Sep. ($''$)	obs. P.A. ($°$)	ϕ_{det}	mV	mH	M/D Sep.	$\theta_{0,FeII}$	$r_{0,FeII}$	$N_e \times N_c \times T_i$
22173-0042	08/17/2011	7.7641±0.0011	30.484±0.014	$0°$	8.5	7.9	$4°$	$8.9''$	0.7 m	$150 \times 7 \times 0.3\,\text{s}$
16242+3702	07/09/2011	8.2308±0.0011	50.887±0.017	$110°$	8.7	7.3	$37°/54°$	$5.0''$	0.5 m	$100 \times 12 \times 0.18\,\text{s}$

Table 1. Binary datasets used for our analysis. For each set we list the name of the binary, the observation date, the separation of the binary, the position angle (P.A.) of the binary relative to the detector y axis, angle of the detector y axis relative to N (ϕ_{det}), V- and H-band magnitudes, angular separation to MASS/DIMM star, average θ_0 and r_0 at the observing wavelength, number of exposures N_e, number of coadds N_c, and integration time T_i. The NIRC2 camera was used with an FeII filter.

3.2 Performance Characterization

Our tests of the prediction of the differential atmospheric effects rests upon the transformation of the empirical PSF at the position of the guide star into an off-axis PSF at the companion location using the algorithm described in §2.1. As a first step, we extract the PSFs at the position of the guide star and the companion with the STARFINDER subroutine `psf_extract`[8] from each individual frame. This step reduces any background that might be present due to imperfect "sky" subtraction. After normalizing the PSFs, we generate a PSF prediction of the off-axis PSF at the position of the companion, given the guide star PSF and the atmospheric MASS/DIMM profile using the code described in §2.3. The input parameters for this step are the C_n^2 profile provided by the MASS/DIMM system, the separation of the binary stars, the wavelength and pixel scale of the observations, the zenith angle, and the time information of the individual frame. The resulting outputs are the predicted PSF at the position of the companion star, the Strehl ratios of the guide star and the predicted off-axis PSF, the Fried parameter, the isoplanatic angle, guide star and predicted off-axis OTFs, and perfect Keck PSF and OTF. Since our binary exposures are relatively short, no attempt is made to average the results over large time intervals. In the upper panels of Figs. 4 and 5, we show examples of the guide star, observed companion PSF, and predicted companion PSF for each dataset. The overall appearance of the companion PSF is reasonably well predicted by the atmospheric model, including many details of the halo structure, though some differences remain.

One simple way to quantitatively evaluate the quality of the prediction is to compare the empirical off-axis Strehl ratio with the predicted Strehl ratio. The lower panels of Figs. 4 and 5 show the Strehl ratio for the guide star, the empirical off-axis Strehl ratio, and the predicted Strehl ratio as functions of frame number. The on- and off-axis Strehl ratios are different by a factor of $\sim$1.5 for both cases, which is consistent with the relatively strong degree of anisoplanatism. On average, the Strehl prediction tracks the empirical data well. Fluctuations in the measured Strehl ratio may arise from the algorithm we currently use for measuring this quantity and the relative insensitivity of the data to the PSF halo. That the modeled companion Strehl ratio generally tracks the observed
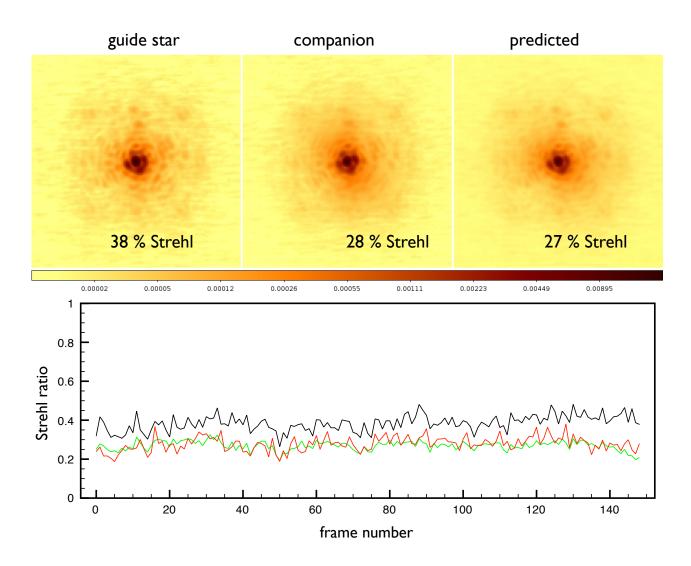
Figure 4. Reconstruction performance for observations of CCDM 22173-0042. The top panel shows extracted guide star, companion, and predicted companion PSFs for an individual frame typical of the dataset. Each subpanel is $1.4''$ on a side. The bottom panel shows the Strehl ratio as a function of frame number for this dataset. The black line shows the Strehl ratio of the guide star, the red is the Strehl ratio of the companion, and the green is the predicted Strehl ratio. These observations were only $4°$ away from the MASS/DIMM guide star.

quantity is encouraging given the larger distance from the telescope to the MASS/DIMM site compared to the Palomar experiment. It is especially encouraging for the case where the binary star is significantly offset from the MASS/DIMM sensing direction, suggesting that reasonable predictions for anisoplanatism may not necessarily be strongly tied to the location of the MASS/DIMM reference star, though this must be further tested.

4. TOWARD ACCOUNTING FOR INSTRUMENTAL PSF VARIATION

Incoming science light will be aberrated by the Keck II telescope, adaptive optics system,[9] and NIRC2 instrument. In general, these aberrations will be a function of field angle. As the system drifts due to flexure in the telescope, thermal variation in the Nasymth-mounted adaptive optics system, and reference centroid location variation with changing Shack-Hartmann wavefront sensor spot size, these aberrations will also change with time. The rms variation of the difference in phase errors between the center and edge of the NIRC2 field can be competitive with anisoplanatic errors in large θ_0 conditions, so proper reconstruction of the off-axis PSF must account
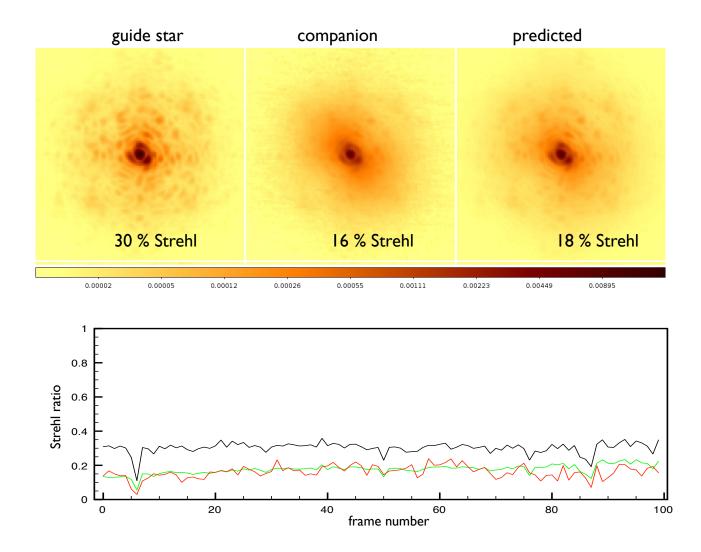
Figure 5. Reconstruction performance for observations of CCDM 16242+3702. The top panel shows extracted guide star, companion, and predicted companion PSFs for an individual frame typical of the dataset. Each subpanel is $1.4''$ on a side. The bottom panel shows the Strehl ratio as a function of frame number for this dataset. The black line shows the Strehl ratio of the guide star, the red is the Strehl ratio of the companion, and the green is the predicted Strehl ratio. The first 29 frames of this observation sequence was $37°$ from the MASS/DIMM guide star, while the remaining frames were $54°$ away.

for instrumental field variation in aberrations in such cases. While the binary star experiments in §3 were performed in low θ_0 conditions where the instrumental contribution to the total field-dependent wavefront error was negligible, the general case must account for field-dependent instrumental aberrations.

We can decompose the time-variable, field-dependent instrumental aberrations into two terms, one containing the contribution to the "on-axis" wavefront (at the reference position $\boldsymbol{\alpha} = 0$), and another characterizing the field dependence,

$$\text{OTF}_{\text{inst}}(\boldsymbol{f}; \boldsymbol{\alpha}, t) = \text{OTF}_{\text{inst-on}}(\boldsymbol{f}; t) \cdot \text{OTF}_{\text{inst-off}}(\boldsymbol{f}; \boldsymbol{\alpha}, t). \quad (2)$$

Here, we presume the differences in the aberrations between positions in the field is independent of time — the only time dependence in the off-axis portion of the instrumental OTF arises from the change in pupil (usually

its orientation),

$$\text{OTF}_{\text{inst}-\text{off}}(\boldsymbol{f};\boldsymbol{\alpha},t) \propto \iint P(\boldsymbol{g};t)P^*(\boldsymbol{g}-\boldsymbol{f};t)\exp\left[i\phi(\boldsymbol{g};\boldsymbol{\alpha})-i\phi(\boldsymbol{g}-\boldsymbol{f};\boldsymbol{\alpha})\right]d\boldsymbol{g}. \tag{3}$$

Here $\phi(\boldsymbol{f},\boldsymbol{\alpha})$ describes the (time-independent) difference in phase aberrations between the reference position and field position $\boldsymbol{\alpha}$. We assume the time-dependent phase aberrations manifest only in the "on-axis" contribution to the instrumental transfer function, $\text{OTF}_{\text{inst}-\text{on}}(\boldsymbol{f};t)$.

The instrumental OTF at the reference position is subsumed into the overall OTF at the reference position, $\text{OTF}_{\text{on}-\text{axis}}(\boldsymbol{f};t)$ in Eq. 1. Therefore, the only remaining pieces needed to described the field variation of the instrumental OTF are the pupil function $P(\boldsymbol{f};t)$ and the difference in phase aberration between the reference position and the field point, $\phi(\boldsymbol{f};\boldsymbol{\alpha})$. We aim to obtain this latter quantity empirically, by means of phase diversity measurements of a steerable fiber source at the Nasmyth focus of the telescope.

We are currently experimenting with using phase diversity measurements to reconstruct the observed fiber PSF. Figure 6 shows a comparison between the observed in-focus PSF and the model PSF constructed from the out-of-focus phase diversity images at a single field position. In general, the Strehl ratio of the modeled PSF is currently recovered to ~10%. While the model PSF constructed from the recovered phase map does not produce a perfect reconstruction of the observed fiber source PSF, the important quantity required for computing $\text{OTF}_{\text{inst}-\text{off}}$ is the relative phase error between field positions, not the absolute value. We plan to use phase diversity measurements obtained in a grid about the NIRC2 narrow camera field of view to construct a model for the variation in the phase aberrations as a function of field position $\phi(\boldsymbol{f};\boldsymbol{\alpha})$. This model can then be combined with the appropriate pupil function to obtain $\text{OTF}_{\text{inst}-\text{off}}(\boldsymbol{f};\boldsymbol{\alpha},t)$.
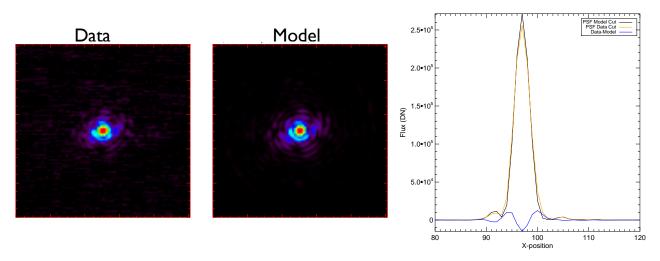

Figure 6. The left panel shows an image of the Nasmyth fiber source being used to probe instrumental contributions to the field-dependent aberrations. The middle panel shows the PSF reconstructed from phase diversity measurements via three out-of-focus images of the fiber source. The rightmost panel shows an x-axis cut of both PSFs and the associated residual. While this comparison serves as a check on our model for the field dependent static wavefront error, it is the difference in phase between field positions that is required for our model. Next steps for modeling $\text{OTF}_{\text{inst}-\text{off}}(\boldsymbol{f};\boldsymbol{\alpha},t)$ include interpolating the phase errors across the field of view.

5. FUTURE EXTENSION TO LASER GUIDE STAR ADAPTIVE OPTICS

A long-term goal of this project is to extend the modeling of the anisoplanatic transfer function to laser guide star operation. We must make additional considerations when seeking to construct a model for this case, particularly in regard to the system geometry and its implications for the stationarity of the structure function. A laser guide star adaptive optics system utilizes light backscattered from a laser beacon for high order wavefront phase compensation and a separate tip/tilt guide star for compensation of wavefront tilt and focus (as well as

aberrations due to the laser guide star). This presents a more complex anisoplanatic configuration than in a natural guide star adaptive optics system. Figure 7 displays a schematic of the LGS configuration. Spherically converging wavefronts from the laser guide star sample a cone of atmospheric turbulence. Plane wavefronts from the tip/tilt guide star and science target sample different cylinders of atmospheric turbulence. The adaptive optics system applies a high order wavefront phase correction measured from the laser beacon wavefront and a tilt phase correction measured from the tip/tilt guide star wavefront. The resulting differential wavefront phase error between the wavefront phase estimate formed from the tip/tilt and laser guide star and the wavefront phase error in the direction of the science target contains contributions from both angular and focal anisoplanatism that depend upon the angular offsets among the laser beacon, tip/tilt guide star, and science target.

As in the natural guide star case, an analytic form for the long exposure atmospheric structure function is available that accounts for the relative location of the stars and laser beacon. Due to the finite altitude of the laser beacon, this structure function is no longer stationary. It is still possible to calculate an optical transfer function from this nonstationary structure function. This OTF depends on the observing wavelength λ, the aperture diameter D, the angular offsets among the laser beacon and/or natural guide stars and the science target, the zenith angle ζ, the vertical turbulence profile $C_n^2(z)$, and the range to laser guide star.

In the center panel of Figure 7 are shown four long exposure PSFs formed by a 10 m circular aperture. The upper left subpanel displays the diffraction limited Airy pattern arising from perfect compensation of the science target. The remaining three subpanels show the long exposure PSF assuming perfect compensation by the tip/tilt guide star and a laser beacon at 90 km. The upper right subpanel shows the case when a 90 km laser beacon, tip/tilt guide star and the science target are all at the same field location. The effect of focal anisoplanatism arising from the finite LGS altitude is to blur the PSF in an axially symmetric fashion. The bottom two images show the effects of displacing the laser beacon and/or tip/tilt guide star by 30″, leading to blurring of the PSF in the direction of the offset. The rightmost panel of Figure 7 shows radial cuts through these four PSFs, which demonstrate the field dependent anisoplanatic degradations arising from atmospheric turbulence. Naturally the LGS adaptive optics PSFs displayed in Figure 7 depend on the vertical distribution of atmospheric turbulence.
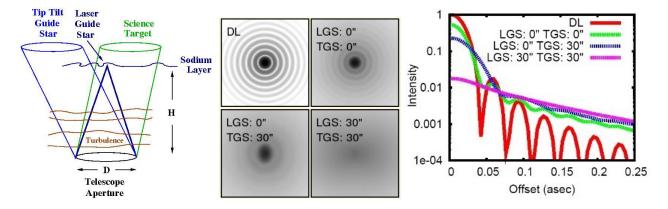

Figure 7. Anisoplanatism in a Sodium Laser Guide Star Adaptive Optics System. At left is shown the conical path traversed by light from the laser beacon (dark blue), and the cylindrical paths traversed by light from the tip/tilt guide star (light blue) and light from the science target (green). At center is shown long exposure PSFs delivered by a diffraction limited 10 m aperture and by a 90 km laser guide star adaptive optics system in which the tip/tilt and laser guide stars have been offset from the science target. At right is shown radial cuts through the long exposure PSFs to illustrate the effects of anisoplanatism on the PSF delivered by a sodium laser guide star adaptive optics system.

The nonstationarity of the long exposure atmospheric structure function has implications for the modeling of the full optical transfer function delivered by the adaptive optics system. Stationarity in the natural guide star case permits the factorization expressed in Equation 1. The loss of stationarity in the LGS adaptive optics geometry requires a more general approach to the prediction of a time and field dependent PSF that accounts for residual aberrations from the adaptive optics system, from instrumental effects, and from the effects of

anisoplanatism arising in atmospheric turbulence. These issues will be addressed by this collaboration in future work.

6. CONCLUSIONS AND SUMMARY OF FUTURE WORK

This project aims to use MASS/DIMM data on Mauna Kea to reconstruct the field-dependent point-spread function for the ultimate goal of improved astrometry in the Galactic Center. We presume the on-axis point-spread function will be measured or otherwise inferred (Jolissaint et al., this volume). We have provided a demonstration of forward modeling of the anisoplanatic transfer function on-sky using MASS/DIMM information on Mauna Kea using observations of visual binary stars in relatively strong anisoplanatism. Given the on-axis PSF of one binary component, we are able to recover the PSF of the binary companion. The predicted Strehl ratio generally tracks the observed Strehl ratio of the companion PSF.

The binary star test cases presented in §3 show that the modeling of atmospheric anisoplanatism (§2) is a powerful tool to predict first order differential effects between guide star and off-axis PSFs. However, the ultimate goal of our model is the prediction of the detailed off-axis PSF. We are working to acquire additional data and improve the observational and analysis methodology. To this end, we will

- conduct other binary star observations to monitor the predictive power of the atmospheric model under different conditions and differing pointings with respect to the MASS/DIMM star.

- characterize the measurement errors related to the algorithm used for Strehl ratio measurement in order to more quantitatively test the prediction of Strehl ratios against the observations. These statistics are important for a comparison of PSFs measured at different signal-to-noise levels, i.e. with different degrees of PSF halo sensitivity.

- apply other metrics than Strehl ratio (e.g. centroid error or encircled energy) in order to provide information on the quality of the prediction that is more relevant to science use cases.

- increase the signal-to-noise of the PSF halo measurements. We must take different binary and fiber-source data with different integration times, potentially saturating the core of the PSF but allowing for reliable mapping the outer structure of the PSF.

- implement an empirical model for the field-dependent instrumental aberrations (§4).

- develop an on-sky observation strategy suited to testing the instrumental differential effects. We will first observe binary stars with smaller separations to measure the instrumental effects between the optical axis and field edges. Image sharpening at the position of the guide star instead of the center position might additionally improve the accuracy of on-sky tests of the instrumental PSF degradation.

As discussed in §5, we are also working to extend the technique to laser guide star operation, which requires additional theoretical development.

ACKNOWLEDGMENTS

REFERENCES

[1] Schödel, R., "Accurate photometry with adaptive optics in the presence of anisoplanatic effects with a sparsely sampled PSF. The Galactic center as an example of a challenging target for accurate AO photometry," *A&A* **509**, A58 (Jan. 2010).

[2] Steinbring, E., Faber, S. M., Hinkley, S., Macintosh, B. A., Gavel, D., Gates, E. L., Christou, J. C., Le Louarn, M., Raschke, L. M., Severson, S. A., Rigaut, F., Crampton, D., Lloyd, J. P., and Graham, J. R., "Characterizing the Adaptive Optics Off-Axis Point-Spread Function. I. A Semiempirical Method for Use in Natural Guide Star Observations," *PASP* **114**, 1267–1280 (Nov. 2002).

[3] Flicker, R. C. and Rigaut, F. J., "Anisoplanatic deconvolution of adaptive optics images," *Journal of the Optical Society of America A* **22**, 504–513 (Mar. 2005).

[4] Britton, M. C., "The Anisoplanatic Point-Spread Function in Adaptive Optics," *PASP* **118**, 885–900 (June 2006).

[5] Tokovinin, A., Baumont, S., and Vasquez, J., "Statistics of turbulence profile at Cerro Tololo," *MNRAS* **340**, 52–58 (Mar. 2003).

[6] Skidmore, W., Schöck, M., Tokovinin, A. A., Djorgovski, G., Walker, A. R., Blum, R. D., Travouillon, T., Seguel, J., Bustos, E. E., Walker, D., Vasquez, J., and Gillett, P. E., "The Thirty Meter Telescope site testing system," *Proc. SPIE* **5489**, 154–164 (Oct. 2004).

[7] *Mauna Kea Weather Center.* http://wxws.ifa.hawaii.edu/current/seeing/.

[8] Diolaiti, E., Bendinelli, O., Bonaccini, D., Close, L. M., Currie, D. G., and Parmeggiani, G., "StarFinder: an IDL GUI-based code to analyze crowded fields with isoplanatic correcting PSF fitting," *Proc. SPIE* **4007**, 879–888 (July 2000).

[9] Wizinowich, P. L., Le Mignant, D., Bouchez, A. H., Campbell, R. D., Chin, J. C. Y., Contos, A. R., van Dam, M. A., Hartman, S. K., Johansson, E. M., Lafon, R. E., Lewis, H., Stomski, P. J., Summers, D. M., Brown, C. G., Danforth, P. M., Max, C. E., and Pennington, D. M., "The W. M. Keck Observatory Laser Guide Star Adaptive Optics System: Overview," *PASP* **118**, 297–309 (Feb. 2006).